Chaos from Orbit-Flip Homoclinic Orbits Generated in a Practical Circuit

Hisa-Aki Tanaka

Department of Electronics and Communication Engineering, Waseda University, Shinjuku-ku, Tokyo 169, Japan

(Received 15 March 1994)

A new class of chaotic systems is generated in a practical, nonlinear, mutually coupled phase-locked loop (PLL) circuit. Theoretical results make it possible to understand experimental results of such PLL's on the onset of chaos using the geometry of the invariant manifolds, while the resultant simple geometry and complex dynamics is expected to have applications in other areas, e.g., power systems or interacting bar magnets. The 1D map projected from a numerically obtained attractor indicates the existence of a piece-wise linear structure having a sensitive dependence on the bifurcation parameter f_{02}.

PACS numbers: 05.45.+b, 84.30.Ng, 84.30.Qi, 84.30.Wp

Much research has been directed at investigating the dynamical behavior occurring when a homoclinic orbit unfolds. Shil'nikov's theorem straightforwardly shows the existence of the Smale horseshoe near a homoclinic orbit under a specific eigenvalue condition of the linearized matrix located at the saddle-focus fixed point [1]. On the other hand, for a homoclinic orbit arising from a saddle fixed point located in a three-dimensional (3D) vector field, studies aimed at elucidating this phenomena have only been carried out primarily from a mathematical standpoint in which the following generic conditions are considered to hold: (1) The homoclinic orbit $\Gamma(t)$ is tangent to the eigendirections e^u and e^s associated with the principal eigenvalues λ^u and λ^s as $t \to \pm\infty$; (2) $\lambda^u \neq |\lambda^s|$; and (3) the stable manifold $W^s(O)$ at O transversely intersects with the two-dimensional (2D) extended unstable manifold $W^{eu}(O)$ along the homoclinic orbit, where $W^{eu}(O)$ is tangent at O to the linear space spanned by e^u and e^s.

Under conditions (1)–(3), nonexistence of homoclinic doubling bifurcation is proven [2]. However, if one of the above conditions is broken, complex dynamical behaviors are known to occur [3–6], namely, the homoclinic orbit is called orbit flip or inclination flip when conditions (1) or (3) are broken, respectively. Results have been obtained regarding the Smale horseshoe in an unfolding of the orbit-flip homoclinic point [4] or inclination-flip homoclinic point [5]. Kokubu and Oka [4] investigated the unfolding of the orbit-flip homoclinic point and demonstrated the existence of the Smale horseshoe and invariant foliation, while Homburg, Kokubu, and Krupa [5] showed in an unfolding of the inclination-flip homoclinic point that N-homoclinic bifurcation occurs under some eigenvalue conditions of the linearized matrix located at the saddle fixed point. Iori's [6] detailed numerical study was the first to confirm such bifurcation for the orbit-flip case using a piecewise linear ordinary differential equation (ODE). However, resultant chaos from the orbit-flip homoclinic orbit has not yet been identified to occur in a concrete system, i.e., one possessing associated chaotic dynamics unfolding from the orbit-flip homoclinic orbit. This led to the present Letter which describes a real, practical system that possesses chaotic behavior for modeling orbit-flip homoclinic bifurcation. In addition, the system's Smale horseshoe generation mechanism is explained.

Throughout this Letter, phase-locked loops (PLL's) are considered that incorporate a voltage controlled oscillator (VCO), a phase detector (PD) having triangular characteristics (Fig. 1), and a loop filter (LF) comprised of a simple RC filter with transfer function $F(S) = 1/(1 + \tau S)$. Such PLL's can be connected to form mutually coupled PLL's, which are frequently used in practical communication systems to synchronize geographically separated timing clocks. The following fourth-order ODE describes the dynamics of the phases of such PLL's:

$$\begin{aligned} &\ddot{x}_1 + 2\zeta_1\dot{x}_1 + h(x_1 - x_2) = \delta\,, \\ &\ddot{x}_2 + 2\zeta_2\sqrt{r_1/r_2}\dot{x}_2 + (r_1/r_2)h(x_2 - x_1) = -(r_1/r_2)\delta\,, \end{aligned} \tag{1}$$

where x_1 and x_2 are normalized variables from phases ϕ_1 and ϕ_2 of PLL 1 and PLL 2, respectively. $\zeta_1, \zeta_2, r_1, r_2$, and δ are also normalized parameters of PLL 1 and PLL 2, while h is a 2π-periodic triangular function (Fig. 1). Equation (1) can be normalized to give

$$\begin{aligned} &\dot{q}_1 = p_1\,, \quad \dot{q}_2 = p_2\,, \\ &\dot{p}_1 = -\beta_1 h(q_1 - q_2) - \alpha_1 p_1 + \gamma_1\,, \\ &\dot{p}_2 = -\beta_2 h(q_2 - q_1) - \alpha_2 p_2 + \gamma_2\,, \end{aligned} \tag{2}$$

where $\alpha_1 = 2\zeta_1$, $\alpha_2 = 2\zeta_2\sqrt{r_1/r_2}$, $\beta_1 = 1$, $\beta_2 = r_1/r_2$, $\gamma_1 = \delta$, and $\gamma_2 = -(r_1/r_2)\delta$.

Mutually coupled PLL's possess chaotic dynamics for a wide range of realistic parameters. Although not synchronized, they are close to synchronization, i.e., they are *marginally* out of lock as described by Endo and Chua [7]. These researchers carried out experiments using

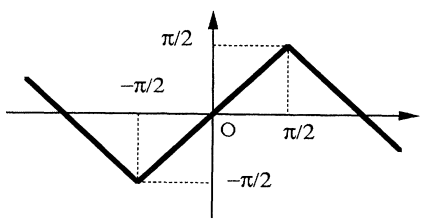

FIG. 1. Triangular phase detector characteristics.

0031-9007/95/74(8)/1339(4)$06.00

real PLL integrated circuit modules as well as performing corresponding numerical simulations. Consequently, they numerically showed the existence of the positive Liapunov exponent, and also described the resultant broadband power spectrum generated by the real circuits.

Physically, Eq. (2) describes a class of mutually coupled nonlinear oscillators with 2π-periodic odd functions. It should be noted that symmetry reduces Eq. (2) to a third-order ODE, namely, by introducing $P_1 = p_1 + p_2$, $P_2 = p_1 - p_2$, $Q_1 = q_1 + q_2$, and $Q_2 = q_1 - q_2$, Eq. (2) becomes

$$\dot{Q}_1 = P_1, \tag{3a}$$

$$\dot{Q}_2 = P_2, \tag{3b}$$

$$\dot{P}_1 = -(\alpha_+ P_1 + \alpha_- P_2)/2 - \beta_- h(Q_2) + \gamma_+, \tag{3c}$$

$$\dot{P}_2 = -(\alpha_- P_1 + \alpha_+ P_2)/2 - \beta_+ h(Q_2) + \gamma_-, \tag{3d}$$

where $\alpha_+ = \alpha_1 + \alpha_2$, $\alpha_- = \alpha_1 - \alpha_2$, $\beta_+ = \beta_1 + \beta_2$, $\beta_- = \beta_1 - \beta_2$, $\gamma_+ = \gamma_1 + \gamma_2$, and $\gamma_- = \gamma_1 - \gamma_2$.

Note the solution for P_1, P_2, and Q_2 can only be determined by Eqs. (3b)–(3d). Next, we employ the transformation $x = P_1/\beta_- - P_2/\beta_+$, $y = P_2/\beta_+$, and $z = Q_2$, which reduces Eq. (3) to the following third-order ODE:

$$\begin{aligned} \dot{x} &= A_1 x + A_2 y, \\ \dot{y} &= B_0 + B_1 x + B_2 y - h(z), \\ \dot{z} &= \beta_+ y, \end{aligned} \tag{4}$$

where $A_1 = (\alpha_-/\beta_+ - \alpha_+/\beta_-)\beta_-/2$, $A_2 = (\beta_-/\beta_+ - \beta_+/\beta_-)\alpha_-/2$, $B_0 = \gamma_-/\beta_+ = \delta$, $B_1 = -\alpha_-\beta_-/2\beta_+$, and $B_2 = -(\alpha_-/\beta_+ + \alpha_+/\beta_-)\beta_-/2$. Although $h(z)$ can be either sinusoidal or triangular depending on the type of employed phase detector, only the triangular function is considered here.

Since Eq. (4) is 2π periodic with respect to z, let us concentrate on the region $D = \{(x, y, z) | -\pi - \delta \le z \le \pi - \delta\}$, in order to examine the geometric structure of the defined vector field. Region D can be divided into three segments, D_+, D_0, and D_-, respectively, defined by $D_+ = \{(x, y, z) | \pi/2 < z \le \pi - \delta\}$, $D_0 = \{(x, y, z) | |z| \le \pi/2\}$, and $D_- = \{(x, y, z) | -\pi - \delta < z < -\pi/2\}$, where the vector field in each segment is linear. Further, denote the planes $\{(x, y, z) | z = \pm\pi/2\}$ as $\sum_+$, and $\sum_-$, respectively. From Eq. (4) and the form of $h(z)$, it follows that a unique equilibrium point at O_+, O_0, O_- exists in D_+, D_0, D_-, with their positions being, respectively,

$$O_\pm = (0, 0, \pm\pi - \delta), \quad O_0 = (0, 0, \delta). \tag{5}$$

Here, attention is focused only on one of the three sets of chaotic parameters experimentally obtained by Endo and Chua [7]:

$$\begin{aligned} &\zeta_1 = 0.614, \quad \zeta_2 = 0.331, \\ &f_{01} = 18\,250 \text{ Hz}, \quad f_{02} = 25\,400 \text{ Hz}, \\ &r_1 = 45\,500/12\,500, \quad r_2 = 5.027/5.298, \\ &\delta = 2\pi(f_{01} - f_{02})/(45\,500 + 12\,500), \end{aligned} \tag{6}$$

leading to

$$\begin{aligned} &A_1 = -1.242\,187, \quad A_2 = -0.038\,378, \\ &B_1 = -0.020\,119, \quad B_2 = -1.282\,425, \\ &B_0 = \delta = -0.774\,565, \quad \beta_+ = 4.836\,228. \end{aligned} \tag{7}$$

The set of parameters in Eq. (7) corresponds to the real eigenvalues λ_s, λ_{ss}, and λ_u of the linearized matrix of the vector fields at O_+ and O_-. These are obtained by solving

$$-\lambda(\lambda - A_1)(\lambda - B_2) + \beta_+(A_1 - \lambda) + A_2 B_1 \lambda = 0, \tag{8}$$

giving $(\lambda_s, \lambda_{ss}, \lambda_u) = (-1.241\,990, -2.932\,221, 1.649\,599)$. In segment D_0, the real eigenvalue λ_1 and the pair of complex-conjugate eigenvalues $\lambda_{2,3}$ are obtained by

$$-\lambda(\lambda - A_1)(\lambda - B_2) + \beta_+(\lambda - A_1) + A_2 B_1 \lambda = 0, \tag{9}$$

giving $(\lambda_1, \lambda_{2,3}) = (-1.242\,387, -0.641\,112\,4 \pm 2.013\,431 i)$. The corresponding eigenvectors (x, y, z) to the above eigenvalues determined the invariant manifolds $W^s(O_-), W^s(O_0), E(O_0)$, and $W^u(O_\pm)$, and the extended unstable manifold $W^{eu}(O_+)$. Figure 2(a) schematically depicts these invariant manifolds, where $W^s(O_-)$ and $W^{eu}(O_+)$ are planes, respectively, spanned by e^s and e^{ss}, or by the eigendirections e^s and e^u, giving the lines $W^s(O_-) \cap \sum_-$ and $W^{eu}(O_+) \cap \sum_+$. From Eqs. (5), (8), and (9), it is evident that the positions of O_+, O_0, and O_- depend only on the parameter δ, and that the eigenvalues (vectors) are not dependent on δ. Hence, if we only change δ, i.e., the free-running angular frequency f_{02} of PLL 2, then $W^s(O_-), W^s(O_0), E(O_0), W^u(O_\pm)$, and $W^{eu}(O_+)$ do not change their normal vectors or directions, though they are shifted in the z direction by the position changes of O_-, O_+, and O_0. Therefore, a critical parameter δ_c is expected to exist under the following situation: (i) The intersecting point p_+ of $\sum_+$ and $W^u(O_+)$ is mapped onto the intersection of $W^s(O_-)$ and $\sum_-$ by the linear flow in D_0 for $\delta = \delta_c$ [Fig. 2(a)]. If $\delta \neq \delta_c$, the following situations are expected to occur depending on whether $\delta < \delta_c$ or $\delta > \delta_c$: (ii) for $\delta > \delta_c$, p_+ is mapped to the half-space containing O_0 separated by $W^s(O_-)$, as shown in Fig. 2(b), or (iii) for $\delta < \delta_c$, p_+ is mapped to the opposite half-space separated by $W^s(O_-)$. Situation (i) leads to a set of two nonlinear (finite dimensional) equations derived from the solution of Eq. (4) in D_0, where f_{02} and the time interval T, in which p_+ is mapped from $\sum_+$ to $\sum_-$, are unknown. By using the parameter values of $f_{01}, \zeta_{1,2}$, and $r_{1,2}$ in Eq. (6), δ_c (i.e., critical frequency $\tilde{f}_{02}$) for situations (i) can be obtained by solving these nonlinear equations, giving

$$\tilde{f}_{02} = 25\,395.327, \quad \tilde{T} = 0.787\,206. \tag{10}$$

From Eqs. (6) and (10), $\delta_c = -0.774\,058$. When $\delta = \delta_c$, the point mapped from p_+ to the intersection of $W^s(O_-)$ and $\sum_-$ asymptotically goes to O_-, because $\lambda_{ss} < \lambda_s < 0$. Thus, situation (i) indicates that a saddle connection exists between O_+ and O_-, as shown in Fig. 2(a). Such a connection can be considered as a homoclinic orbit if O_+ and O_- are identified. When δ is slightly larger than δ_c, the orbits from the neighborhood of p_+ go to the

sink O_0, i.e., the two PLL's undergo lock-in as shown in Fig. 2(b). However, when δ is slightly less than δ_c, being the case if the set of parameters are per Eq. (7), this situation can be considered to represent an unfolding of the orbit-flip homoclinic point as shown in Fig. 2(c). Solving a set of two nonlinear equations having unknown variables f_{02} and T in a similar manner as that mentioned above, the orbit-flip homoclinic point can be verified to exist at the slightly different parameters of $A_2 = 0$ and $B_0 = -0.774\,348$, while $A_1, \ldots, B_2$ and β_+ are the same as in Eq. (7). In this case, the saddle connection exists in the plane $x = 0$. Since Eq. (4) is linear in D_0, the transversality of $W^{eu}(O_+)$ and $W^s(O_-)$ along the saddle connection can be verified by solving the variational equation along the saddle connection in D_0. Hence, Eq. (7) is the parameter set that represents unfolding of the orbit-flip homoclinic point. This behavior completely explains that shown experimentally, i.e., chaos occurs in a *marginal* out-of-lock condition [7].

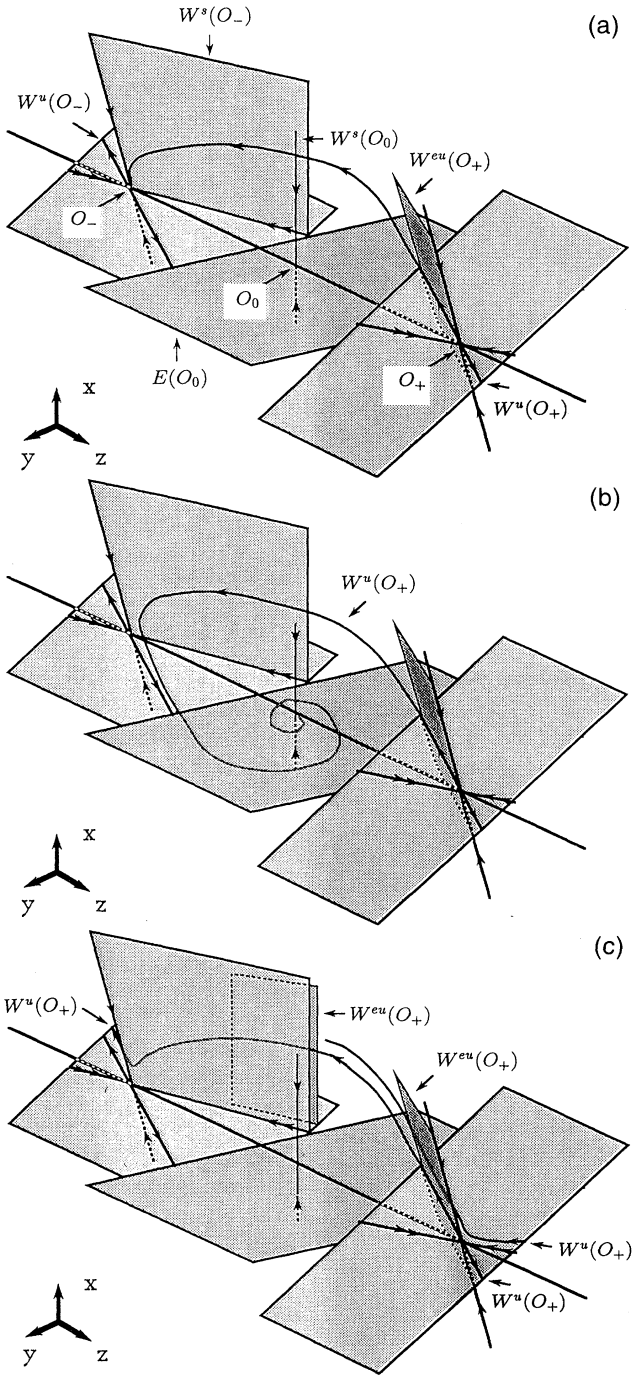

FIG. 2. (a) Saddle connection in the piecewise linear flow. (b) Lock-in dynamics for $\delta > \delta_c$. (c) Out-of-lock dynamics for $\delta < \delta_c$.

The existence of the Smale horseshoe arising from an orbit-flip homoclinic orbit in the general system [4] can be proven. Figure 3 illustrates the generation mechanism of the Smale horseshoe arising from Eq. (4). By identifying O_+ and O_-, we can explicitly obtain two flow-defined maps $\prod_1 : \sum_+ \to \sum_-$ and $\prod_2 : \sum_- \to \sum_+$ in the neighborhood of the original homoclinic orbit. $\prod_1$ is shown to be a diffeomorphism approximated by a linear map in the neighborhood of the homoclinic orbit, while an analysis of the solution in $D_\pm$ will show $\prod_2$ produces a folding effect. Therefore, $\prod_2 \circ \prod_1$ folds a small rectangle on $\sum_+$ near the homoclinic orbit and maps back the folded object onto the original rectangle on $\sum_+$: a behavior proving the Smale horseshoe exists in a suitably chosen, small, thin region near the original homoclinic orbit. Moreover, a one-periodic orbit is expected to appear along the original homoclinic orbit [8], and can be verified to exist with the parameter set of Eq. (7) using a computer-assisted proof based on self-validated numerics. Using the parameters of Eq. (7), we numerically obtained the cross section at $\sum_-$, using a detailed double-precision computation; thereby showing the occurrence of a small, thin attractor [Fig. 4(a)] that appears to have a piecewise linear structure in an affine transformed coordinate of x and y. To examine the dynamics occurring on the at-

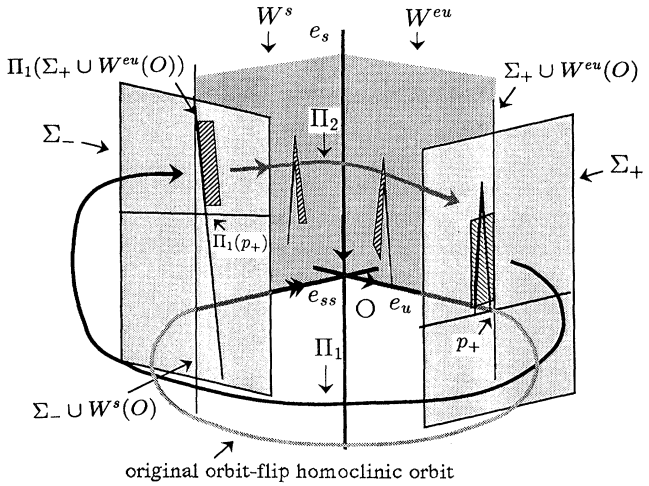

FIG. 3. Mechanism of generating the Smale horseshoe.

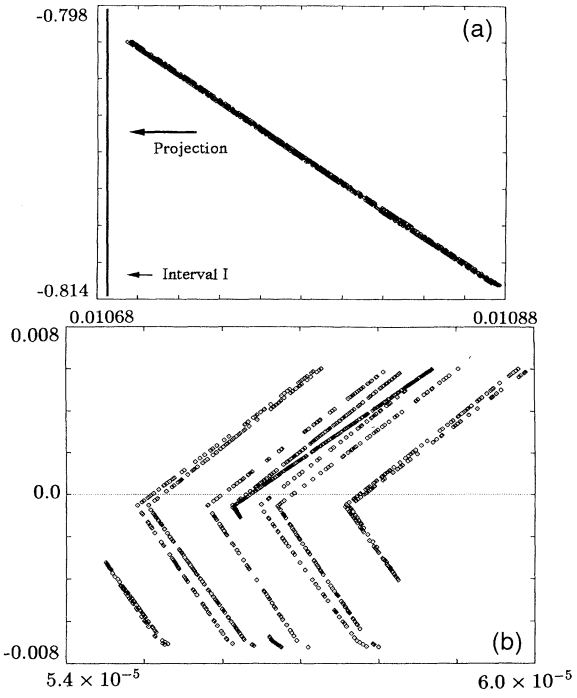

FIG. 4. A cross section of the attractor at $\sum_-$, in the original coordinate for $f_{02} = 25\,400$ Hz. (b) A cross section of the same attractor at $\sum_-$, in an affine transformed coordinate of x and y for $f_{02} = 25\,400$ Hz.

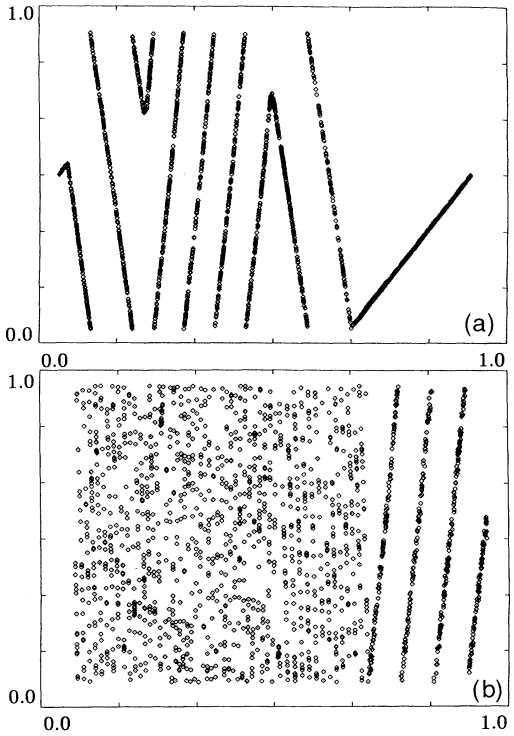

FIG. 5. One-dimensional map from the attractor near the orbit-flip homoclinic orbit for various f_{02} values. (a) $f_{02} = 25\,400$ Hz and (b) $f_{02} = 25\,396$ Hz.

tractor, we analyzed a one-dimensional (1D) map numerically obtained by a projection from the attractor to the interval $I:[-0.814, -0.798]$ depicted in Fig. 4(a). Of interest is that the numerically obtained 1D map $I \rightarrow I$ can be well fitted using a piecewise linear discontinuous function, in which I was rescaled to [0.0,0.1] (Fig. 5). The reason why such piecewise linearity occurs is now under investigation. Figures 5(a)–5(b), respectively, show the resultant 1D maps for $f_{02} = 25\,400$ and $25\,396$ Hz. As f_{02} decreases to $\tilde{f}_{02}$, the 1D map explosively grows finer [Fig. 5(b)]. Such rapid growth in the complexity of the 1D map near $\tilde{f}_{02}$ (i.e., δ_c) coincides with the rapid increase of the maximum Liapunov exponent as f_{02} decreases to $\tilde{f}_{02}$ [7].

In summary, this Letter reports the discovery of a new class of chaotic dynamics arising from the orbit-flip homoclinic orbit generated by a practical nonlinear, mutually coupled PLL circuit, while also providing an explanation as to why chaos occurs in a *marginal out-of-lock* condition [7]. Because the system's governing equation and the resultant geometry of the vector field are simplistic, its use it expected to lead to novel results when applied to systems in other fields, e.g., a two-generator power system modeled by the swing equations [9], or two interacting bar magnets confined to a plane (see [10] for the simplified overdamped case).

Sincere gratitude is extended to Professor S. Oishi and Professor K. Horiuchi, Waseda University, for their valuable comments, and also to Professor T. Endo, Meiji University; Professor H. Kokubu, Kyoto University; Professor T. Matsumoto, Waseda University; and Professor S. H. Strogatz, Cornell University for their beneficial discussions. This work was completed at the workshop "Various Approach to Complex Systems," held at the international Institute for Advance Studies (Kyoto-Osaka-Nara, Japan) in 1994.

[1] L. P. Shil'nikov, Sov. Math Dokl. **6**, 163 (1965).
[2] J. W. Evans, N. Fenichel, and J. A. Feroe, SIAM J. Appl. Math. **42**, 219 (1982).
[3] E. Yanagida, J. Diff. Eq. **66**, 243 (1987).
[4] H. Kokubu and H. Oka (to be published).
[5] A. J. Homburg, H. Kokubu, and M. Krupa (to be published).
[6] K. Iori, E. Yanagida, and T. Matsumoto, in *Structure and Bifurcations of Dynamical Systems*, edited by S. Ushiki, Advanced Series in Dynamical Systems Vol. 11 (World Scientific, Singapore, 1993), p. 82.
[7] T. Endo and L. O. Chua, IEEE Trans., CAS Vol. 37, No. 9, 1183 (1990).
[8] M. Kisaka, H. Kokubu, and H. Oka, J. Dynam. Diff. Eq. **5**, 305 (1993).
[9] F. M. A. Salam, J. E. Marsden, and P. P. Varaiya, IEEE Trans., CAS, Vol. 31, No. 8, 673 (1984).
[10] S. H. Strogatz, *Nonlinear Dynamics and Chaos* (Addison-Wesley, Massachusetts, 1994), p. 286.

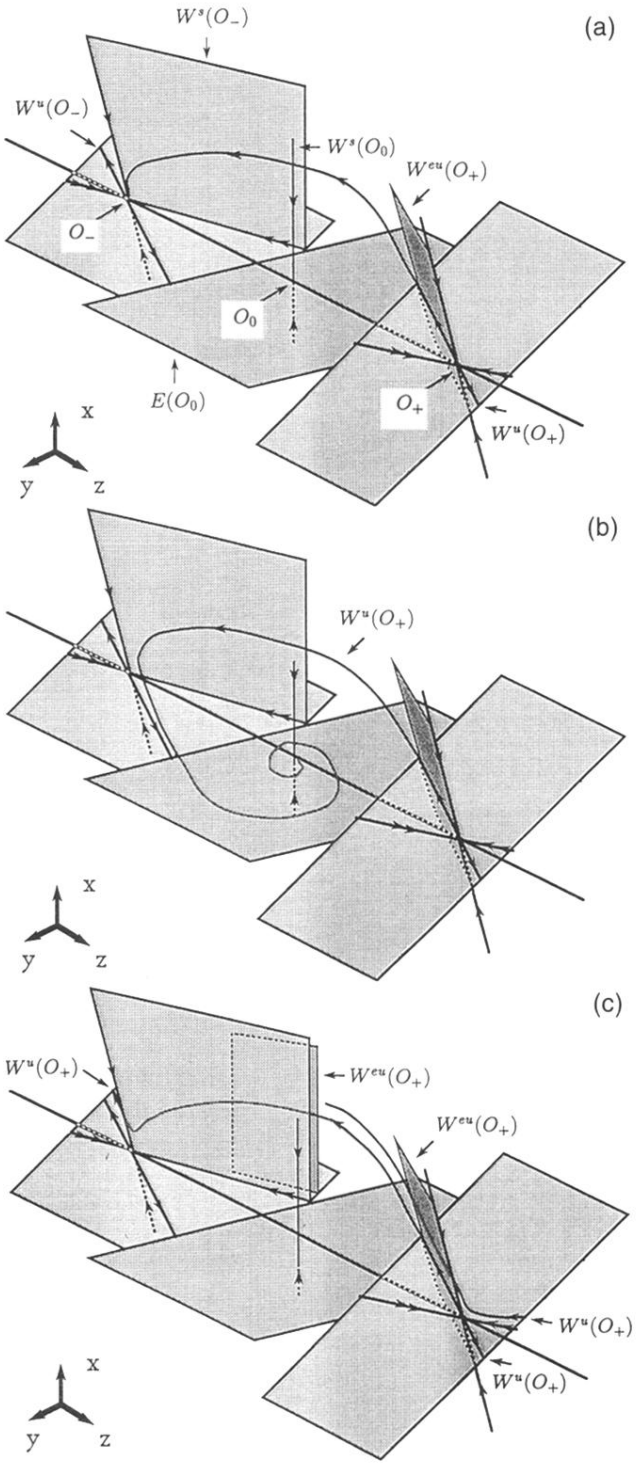

FIG. 2. (a) Saddle connection in the piecewise linear flow. (b) Lock-in dynamics for $\delta > \delta_c$. (c) Out-of-lock dynamics for $\delta < \delta_c$.

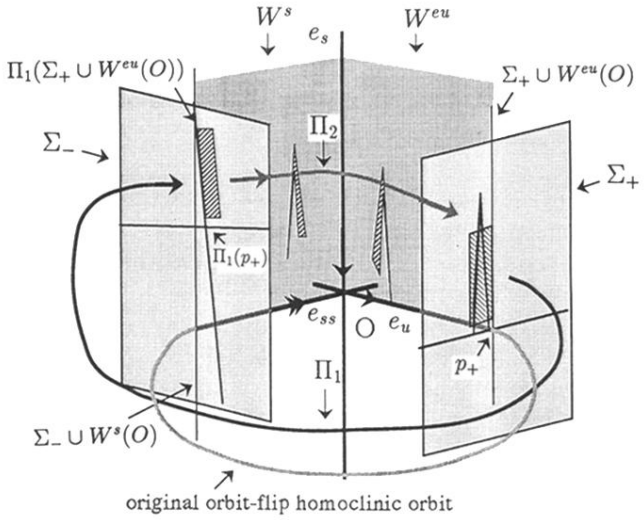

FIG. 3. Mechanism of generating the Smale horseshoe.